INTERNATIONAL JOURNAL OF PRECISION ENGINEERING AND MANUFACTURING Vol. 15, No. 1, pp. 53-61 JANUARY 2014 / 53
DOI: 10.1007/s12541-013-0305-6

Design of Test Track for Accurate Calibration of Two Wheel Differential Mobile Robots

Changbae Jung[1], Chang-bae Moon[1], Daun Jung[1], JongSuk Choi[2], and Woojin Chung[1,#]

1 School of Mechanical Engineering, Korea University, Anam-dong, Seongbuk-gu, Seoul, South Korea, 136-713
2 Center for Bionics, Biomedical Engineering Research Institute, Korea Institute of Science and Technology, Hawolgok-dong 39-1, Seongbuk-gu, Seoul, South Korea, 136-791
Corresponding Author / E-mail: smartrobot@korea.ac.kr, TEL: +82-2-3290-3375, FAX: +82-2-3290-3375

KEYWORDS: Mobile robot, Calibration, Odometry, Localization

Odometry using incremental wheel encoder sensors provides the relative position of a mobile robot. The major drawback of odometry is the accumulation of kinematic modeling errors when travel distance increases. The major systematic error sources are unequal wheel diameters and erroneous wheelbase. The UMBmark test is a practical and useful calibration scheme for systematic odometry errors of two wheel differential mobile robots. We previously proposed an accurate calibration scheme that extends the conventional UMBmark. A calibration experiment was carried out using the robot's heading errors, and kinematic parameters were derived by considering the coupled effect of the systematic errors on a test track. In this paper, we propose design guidelines of test tracks for odometry calibration. As non-systematic errors constitute a grave problem in practical applications, the test track shape and size should be determined by considering the distributions of systematic and non-systematic errors. Numerical simulations and experiments clearly demonstrate that the proposed scheme results in more accurate calibration results.

Manuscript received: May 21, 2013 / Accepted: November 18, 2013

1. Introduction

Recently, various researches for autonomous navigation are being carried out.[1-4] Autonomous navigation requires accurate estimation of the position of a mobile robot. The most common relative positioning technique for mobile robots is odometry using a wheel encoder. However, odometry has a well-known drawback: kinematic modeling errors accumulate as the robot's travel distance increases. Calibration is necessary to reduce the odometry errors that occur with increased travel distance. Improved odometry can significantly reduce the operational costs associated with the installation and maintenance of sensors and landmarks. It also reduces the uncertainty of the estimated pose (position and orientation) when external sensors cannot be used because of weather or environmental conditions. The extended Kalman filter (EKF) assumes that the mean of the added Gaussian noise in state transition is zero.[5] For that reason, the EKF based localization technique is useful when the odometry has a zero mean and white Gaussian noise.

Odometry error sources can be classified as systematic and non-systematic errors.[5-7] Systematic errors are vehicle-specific and do not usually change abruptly during navigation. Therefore, systematic errors can be reduced by calibrating the kinematic parameters. Examples of systematic errors include unequal wheel diameters, erroneous wheelbase.

Non-systematic error sources are caused by interactions between the robot and road conditions, which are stochastic. Examples include uneven floors, unexpected objects on the floor, and wheel slippages. External sensors can be added to model the uncertainty of non-systematic errors by using the absolute position of the robot obtained from external sensors.[8-10]

In previous researches, it is difficult to find the design guideline of the test track. The UMBmark method is a useful calibration scheme for two-wheel differential mobile robots.[6] The wheel diameter and wheelbase errors can be calibrated by driving the robot along a bidirectional 4 m × 4 m square path and then measuring the position errors between the initial and final positions. However, test track design was not explicitly explained. Since the size of the test track is important, it should be carefully determined by considering the wheel diameter, calibration equations, kinematic modeling errors, and experimental conditions. The work of Martinelli presented a method for modeling and evaluating the odometry error for a synchronous drive robot.[11] The odometry error is modeled by introducing four parameters characterizing the systematic and nonsystematic components (translational and rotational). Martinelli et al. also proposed the method for estimating odometry error during

© KSPE and Springer 2014

navigation based on augmented Kalman filter (AKF) and Observable filter (OF).[12] Antonelli et al. proposed the calibration schemes to identify a 4-parameter odometry model by using the least-square method.[13] Due to the fact that the odometry model shows the linear relation between the unknowns and the measurements, the use of the least-square method is available. Some guidelines were proposed for choosing test trajectories in which the value of odometry error is normalized using the least-squares approach with respect to the travel distance. The linear estimation approach is further improved by estimating the physical odometry parameters, thus 3-parameter model is yielded.[14] Censi et al. and Antonelli et al. proposed the method for calibrating both odometry and location of sensors with respect to the robot frame at the same time.[15,16]

We previously proposed a calibration scheme for systematic errors that uses the experimental heading errors of the robot's final pose in a test track.[17] The systematic errors can be calibrated by measuring the orientation of the robot after a sequence of open-loop motions along the test track. This method is advantageous because the robot orientation can be measured by an onboard gyroscope. There is no need to install any absolute positioning sensor. As a consequence, the odometry can also be calibrated in outdoor environments.

In this paper, we propose design guidelines of the test track for calibration experiments in order to improve the accuracy of odometry calibration. A significant factor for odometry calibration is the design of the test track. Calibration accuracy can be remarkably improved by using an appropriate test track. It is required that the final pose error should contain the effects from multiple error sources. For examples, the test track should include both straight line motion and spot turning motion in order to monitor the effects from unequal wheel diameters as well as erroneous wheelbase.

This paper is organized as follows. In Section 2, we introduce an odometry error model and problem statements. The proposed design guidelines of the test track are explained in Section 3. In Section 4, the advantages of the proposed design are shown by simulation results. Experimental verifications are shown in Section 5. Finally, concluding remarks are given in Section 6.

2. Odometry Error Model And Error Propagation

The velocity model of a two-wheeled differential mobile robot is presented in Fig. 1. The position and orientation of the robot at time t are given by (x_t, y_t, θ_t). The translational and rotational velocities at time t are denoted by v_t and ω_t, respectively. Two dominant systematic errors are the wheel diameter error and wheelbase error. Translational errors were assumed to be caused by wheel diameter errors $\varepsilon_{r_{R(L)}}$, and rotational errors were assumed to be caused by wheelbase error ε_b. The velocity motion model of a robot is derived from (1) and (2).

$$v_t = \frac{v_R + v_L}{2} = \frac{(r_R + \varepsilon_{r_R}) \cdot \omega_R + (r_L + \varepsilon_{r_L}) \cdot \omega_L}{2} \tag{1}$$

$$\omega_t = \frac{v_R - v_L}{b} = \frac{(r_R + \varepsilon_{r_R}) \cdot \omega_R - (r_L + \varepsilon_{r_L}) \cdot \omega_L}{b_{nom} + \varepsilon_b} \tag{2}$$

where v_R is the translational velocity of the right wheel, v_L is the translational velocity of the left wheel, ω_R is the angular velocity of the right wheel, and ω_L is the angular velocity of the left wheel.

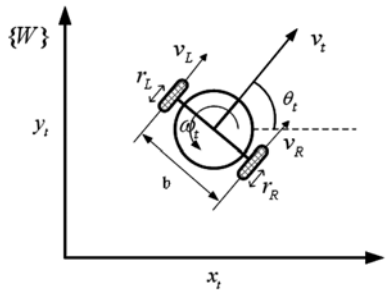

Fig. 1 The velocity model and parameters of a two-wheel differential mobile robot

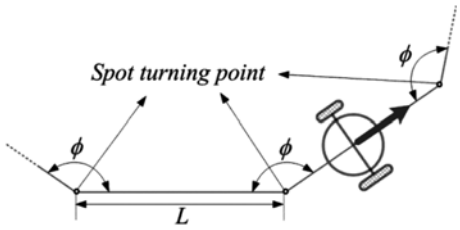

Fig. 2 Test track condition can be generalized in a regular polygon

In order to investigate the error propagation of odometry, we used the velocity motion model of a two-wheel differential mobile robot. The two dominant systematic errors are unequal wheel diameters and incorrect wheelbase. The odometry of a two-wheel differential mobile robot is based on integration of the following equations. v_t and ω_t are given in (1)-(2).

$$\begin{aligned} \dot{x} &= v_t \cdot \cos\theta \\ \dot{y} &= v_t \cdot \sin\theta \\ \dot{\theta} &= \omega_t \end{aligned} \tag{3}$$

The systematic errors of odometry can be calibrated by measuring the robot's final pose errors after open-loop motions along a predefined test track. The test track is required to include the straight-line and spot-turning paths. Also, the initial and final position of the test track should be identical. These conditions can be generalized in a regular polygon shown in Fig. 2. In Fig. 2, L is a length of one straight line and ϕ is an angle between neighboring lines.

After the robot is driven along a regular polygon path, the position and orientation errors (x_e, y_e, θ_e) caused by the kinematic error parameters ε_b, $\varepsilon_{r_{R(L)}}$ are derived using (3).

$$\begin{bmatrix} \dot{x}_e \\ \dot{y}_e \\ \dot{\theta}_e \end{bmatrix} = \begin{bmatrix} \frac{\partial \dot{x}}{\partial \varepsilon_b} & \frac{\partial \dot{x}}{\partial \varepsilon_{r_R}} & \frac{\partial \dot{x}}{\partial \varepsilon_{r_L}} \\ \frac{\partial \dot{y}}{\partial \varepsilon_b} & \frac{\partial \dot{y}}{\partial \varepsilon_{r_R}} & \frac{\partial \dot{y}}{\partial \varepsilon_{r_L}} \\ \frac{\partial \dot{\theta}}{\partial \varepsilon_b} & \frac{\partial \dot{\theta}}{\partial \varepsilon_{r_R}} & \frac{\partial \dot{\theta}}{\partial \varepsilon_{r_L}} \end{bmatrix} \cdot \begin{bmatrix} \varepsilon_b \\ \varepsilon_{r_R} \\ \varepsilon_{r_L} \end{bmatrix} \tag{4}$$

$$\dot{x}_e = \frac{\partial \dot{x}}{\partial \varepsilon_b}\varepsilon_b + \frac{\partial \dot{x}}{\partial \varepsilon_{r_R}}\varepsilon_{r_R} + \frac{\partial \dot{x}}{\partial \varepsilon_{r_L}}\varepsilon_{r_L} = \left(v_t \cdot \sin\theta \cdot \frac{\theta}{b + \varepsilon_b}\right) \cdot \varepsilon_b \tag{5}$$

$$+\left(\frac{\omega_R}{2} \cdot \cos\theta - v_t \cdot \sin\theta \cdot \frac{\omega_R}{b + \varepsilon_b}\right) \cdot \varepsilon_{r_R} + \left(\frac{\omega_L}{2} \cdot \sin\theta - v_t \cdot \cos\theta \cdot \frac{\omega_L}{b + \varepsilon_b}\right) \cdot \varepsilon_{r_L}$$

$$\dot{y}_e = \frac{\partial \dot{y}}{\partial \varepsilon_b}\varepsilon_b + \frac{\partial \dot{y}}{\partial \varepsilon_{r_R}}\varepsilon_{r_R} + \frac{\partial \dot{y}}{\partial \varepsilon_{r_L}}\varepsilon_{r_L} = \left(-v_t \cdot cos\theta \cdot \frac{\theta}{b+\varepsilon_b}\right)\cdot \varepsilon_b \tag{6}$$

$$+\left(\frac{\omega_R}{2}\cdot sin\theta + v_t \cdot cos\theta \cdot \frac{\omega_R}{b+\varepsilon_b}\right)\cdot \varepsilon_{r_R} + \left(\frac{\omega_L}{2}\cdot sin\theta - v_t \cdot cos\theta \cdot \frac{\omega_L}{b+\varepsilon_b}\right)\cdot \varepsilon_{r_L}$$

$$\dot{\theta}_e = \frac{\partial \dot{\theta}}{\partial \varepsilon_b}\varepsilon_b + \frac{\partial \dot{\theta}}{\partial \varepsilon_{r_R}}\varepsilon_{r_R} + \frac{\partial \dot{\theta}}{\partial \varepsilon_{r_L}}\varepsilon_{r_L} \tag{7}$$

$$= \left(-\frac{\omega_t}{b+\varepsilon_b}\right)\cdot \varepsilon_b + \left(\frac{\omega_R}{b+\varepsilon_b}\right)\cdot \varepsilon_{r_R} + \left(-\frac{\omega_L}{b+\varepsilon_b}\right)\cdot \varepsilon_{r_L}$$

Eq. (7) shows that the orientation errors in straight-line and spot-turning paths increase linearly in correspondence to the distance traveled and turning angle. The final orientation errors are clearly equal after runs with the same straight-line length and spot-turning angle without regard to the shape of the test track.

3. Design of Test Tracks

3.1 Problem statements

Jung's method is based on the heading errors of the final robot pose and considers the coupled effect of the simultaneous occurrence of wheelbase and wheel diameter errors. Calibration experiments are carried out by using bidirectional *CW* and *CCW* test motions along the reference test track to compensate for the concealed error of the unidirectional test motion. The kinematic parameters of unequal wheel diameters and incorrect wheelbase can be calibrated simultaneously by using the final pose errors of a robot on a test track.

The main goal of this paper is to propose design guidelines of a test track so that the systematic errors accurately reflect the pose errors. The shape of the test track is required to consist of straight-line and spot-turning paths. The initial and final position of the test track should be identical. It is desirable to maximize the effect of the systematic error on the pose errors for efficient calibration.

The size of the test track should be designed to maximize the final pose errors caused by systematic errors compared with those caused by non-systematic errors. When the track is too large, a huge experimental space is required. In addition, the final pose can be affected by various non-systematic error sources. On the other hand, overly small tracks may result in final pose errors that are too small, which implies that the calibration results are too sensitive with respect to the measurement accuracy of the robot pose. The performance index of a track size is defined as the relative size of the pose errors caused by systematic errors compared with those caused by non-systematic errors.

3.2 Shape of test tracks

Jung's method uses heading errors of the final pose. The final heading angles of a robot are identical after the same path length and turning angles of different path types are followed, as shown in (7). Furthermore, the initial and final positions of the test track should be identical in order to reduce the measurement error of the sensors. Therefore, the shape of the test track is recommended to be a regular polygon path. The proposed test track was designed as a square path in consideration of the available experimental space.

3.3 Size of test tracks

Once the shape of the test track is established, the track size should be carefully determined based on the test space, wheel diameter, calibration equations, and relative magnitude between systematic and non-systematic errors. Although the heading errors of the robot were calculated without approximations by using Jung's method, too long tracks are not preferable. This is due to the increase of non-systematic errors with the distance traveled. The final pose errors caused by systematic errors should be larger than the pose errors by non-systematic errors.

In practical implementation, the robot pose can be estimated by discrete version of (3).

$$x_{t+1} = f(x_t, u_t, t)$$

$$x_{t+1} = \begin{bmatrix} x_{t+1} \\ y_{t+1} \\ \theta_{t+1} \end{bmatrix}, \quad f(x_t, u_t, t) = \begin{bmatrix} x_t + \Delta s \cdot cos(\theta_t + \Delta\theta/2) \\ y_t + \Delta s \cdot sin(\theta_t + \Delta\theta/2) \\ \theta_t + \Delta\theta \end{bmatrix} \tag{8}$$

$$\Delta s = \frac{\Delta s_r + \Delta s_l}{2}, \quad \Delta\theta = \frac{\Delta s_r - \Delta s_l}{b}$$

where Δs is the translational displacement of the robot, $\Delta\theta$ is the rotational displacement of the robot, Δs_r and Δs_l are the distance traveled by each wheel and b is the wheelbase of the robot.

Then, non-systematic errors can be estimated using the following equations.[3]

$$\mathbf{P}_{t+1}^{-} = \mathbf{F}_t \mathbf{P}_t \mathbf{F}_t^T + \nabla_u \mathbf{f} \cdot \Sigma_u \cdot \nabla_u \mathbf{f}^T \tag{9}$$

where $\mathbf{F}_t$ and $\nabla_u \mathbf{f}$ are the *Jacobians* of the robot pose estimation function $f(x_t, u_t, t)$ in (8).

The covariance matrix P_{t+1} represent the stochastic non-systematic errors caused by interactions between the robot and floor conditions. In (9), the first term is related to uncertainties of the estimated state, and the second term is related to odometry errors. For the incremental motion of the left and right wheel, the covariance matrix Σ_u is defined as follows:

$$\Sigma_u = \begin{bmatrix} k_r|\Delta s_r| & 0 \\ 0 & k_l|\Delta s_l| \end{bmatrix} \tag{10}$$

where k_r and k_l are error constants representing the stochastic parameters of the robot and environment interaction.

To investigate the effect of non-systematic errors on the size of the test track, the non-systematic errors were estimated from the experimental results. The error constants of k_r and k_l can be calculated by using the test method.[18]

3.4 Proposed design guidelines

The proposed design guidelines for test tracks can be summarized as follows:

1) Determine the shape of a test track that is composed of straight lines and spot-turning points.

2) Drive the robot along a predefined test track by open-loop motion to estimate the kinematic parameters of an uncalibrated wheelbase and unequal wheel diameters.

3) Measure the non-systematic errors using the test method.[14]

4) Estimate the absolute orientation errors caused by the systematic and non-systematic errors through simulations.

5) Determine the size of the test track to distinguish the systematic errors from the non-systematic errors.

4. Simulations

The objective of the numerical simulations was to establish the design guidelines for the test track. In the simulations, the test track was a square path in consideration of the available experimental space. A two-wheel differential mobile robot (TETRA-DS II) was used to model the simulated robot platform.[19] The nominal wheel dimensions were as follows: *wheel diameter* = 150 *mm*, *wheelbase* = 385 *mm*, and *wheel width* = 30 *mm*. The nominal wheel diameter and wheelbase of the robot were identical to that of the simulated robot. The actual robot position and orientation in the simulations were numerically computed from the robot kinematics while considering the kinematic modeling errors.

The kinematic modeling errors of the wheels were assumed to set the parameter values, E_b and E_d, used in the simulation. E_b and E_d are defined as follows.[6]

$$E_b = \frac{b_{actual}}{b_{nominal}}, \quad E_d = \frac{D_R}{D_L} \tag{11}$$

where b_{actual} is the actual wheelbase of the robot, $b_{nominal}$ are nominal wheelbase of the robot, D_R is the actual wheel diameter of the right wheel, and D_L is the actual wheel diameter of the left wheel.

Non-systematic errors were modeled using the error constants k_r and k_l; the covariance matrix in (10) was then estimated. To investigate the effect of non-systematic errors on the orientation errors caused by systematic errors, the relative error magnitudes were calculated.

The initial parameters for the systematic errors were set to E_b = 0.990 and E_d = 0.995. Non-systematic errors were given with the error constants $k_r^{1/2} = 0.001m^{1/2}$ and $k_l^{1/2} = 0.001m^{1/2}$ under general floor conditions. The track sizes were tested at $L \le 4m$ in consideration of the available experimental space. The actual robot pose errors were numerically computed from the robot kinematics while considering the kinematic modeling errors.

Fig. 3 shows the estimated orientation errors caused by systematic and non-systematic errors on the straight-line path in the test track. The *x*-axis represents the length of one side of the square path. The orientation errors increased with the distance traveled. Fig. 3 shows that the maximum orientation error caused by the systematic and non-systematic errors was 3.43° at 4*m*.

In practical application, the orientation errors caused by systematic errors should be larger than the orientation errors of non-systematic errors. The actual orientation error on the test track was the sum of the orientation errors caused by systematic and non-systematic errors. Therefore, the straight-line length of the test track can be designed by considering the relative magnitudes of the orientation errors caused by the systematic and non-systematic errors.

Fig. 4 shows the relative magnitudes of the orientation error caused by systematic errors to the total orientation error, which is the sum of the orientation errors caused by systematic and non-systematic errors. The relative orientation error caused by systematic errors over the total error increased with the straight-line length. Therefore, the appropriate size of the test track was $4m \times 4m$ under the simulated conditions. When

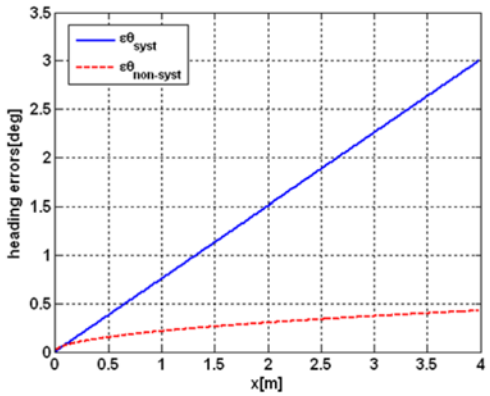

Fig. 3 The orientation errors caused by systematic errors and non-systematic errors of the straight line path in test track

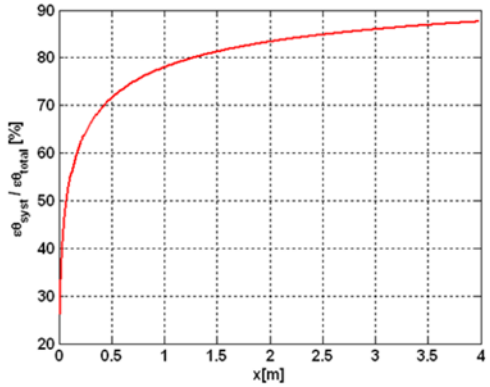

Fig. 4 The relative size of orientation errors caused by systematic errors compared with total orientation errors of the straight line path in test track

the track size is too small, the calibration accuracy decreases due to the possible occurrence of relatively large non-systematic errors.

Fig. 5 shows the mean and standard deviation of the final position errors after runs along the same $4m \times 4m$ square path in *CCW* direction. The final position errors differed after calibrations using different track sizes. The test was repeated five times. The actual kinematic parameters were E_b = 0.975 and E_d = 0.992. The kinematic parameters were then estimated from the different square path tracks. From Fig. 5, it is clear that the final pose error of the $0.5m \times 0.5m$ track was largest. The final pose error decreased until $4m \times 4m$ track. There are no significant change changes in the final pose error when the dimension ranges from 4~10*m*. Therefore, it can be concluded that it is reasonable to choose $4m \times 4m$ track, because the track shows satisfactory calibration accuracy without occupying too large experimental space.

Fig. 5 shows experimental comparison on the basis of sample distributions. Therefore, it is no sufficient enough to show that the error mean of the proposed track is smaller than other cases. It is interesting to investigation whether any meaningful improvement can be achieved by $4m \times 4m$ track design. Statistical analysis was carried out using the independent samples *t-test* to verify significant differences between the means of the final position errors.[20]

Table 1 shows the independent samples *t-test* results of the final position errors for the equality of means of the proposed method ($4m \times$

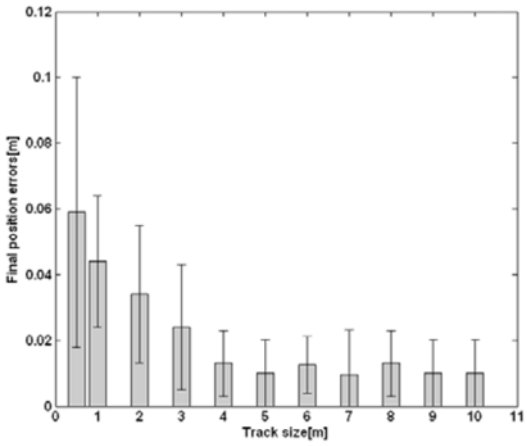

Fig. 5 Simulation results of experimental final position errors when the robot is driven along 4m × 4m square paths in *CCW* direction. Calibrations were carried out under different test track dimensions that are represented in *x* axis

Table 1 Results of independent samples *t-test* for equality of means of the proposed method ($4m \times 4m$) against that of different

Case	t-value	Degree of freedom	p	Mean difference
0.5m × 0.5m vs. 4m × 4m	4.962	21.44	0.000	0.047
1m × 1m vs. 4m × 4m	6.252	28.36	0.000	0.032
2m × 2m vs. 4m × 4m	4.161	38	0.000	0.022
3m × 3m vs. 4m × 4m	2.440	38	0.019	0.012
8m × 8m vs. 4m × 4m	0.146	38	0.885	0.001

$4m$) against those for the $0.5m \times 0.5m$, $1m \times 1m$, $2m \times 2m$, $3m \times 3m$, and $8m \times 8m$ track sizes. As shown in Table 1, the mean of the final position errors with the proposed method ($4m \times 4m$) was different from the means for $0.5m \times 0.5m$, $1m \times 1m$, $2m \times 2m$, and $3m \times 3m$ track sizes at a significance level of 0.05 ($p < 0.05$). This fact implies that the resultant sample distributions of the upper 4 rows of Table 1 are stochastically different. Therefore, it can be concluded that the proposed $4m \times 4m$ track design resulted in meaningfully smaller pose error distribution over other cases.

On the other hand, significance level p of the bottom row was 0.885 > 0.05. This fact implies that it is difficult to say that the resultant distributions between the proposed $4m \times 4m$ track design and $8m \times 8m$ track design show meaningful difference. In other word, two sample distributions are similar. Therefore, $4m \times 4m$ track is preferable because of smaller experimental space.

5. Experimental Results

Experiments consist of two parts. In the first experiment, it was investigated whether the test track that designed along the proposed guideline is advantageous in the practical environment. Experimental results using three different test tracks were presented. In the second experiment, a proposed scheme was compared with the conventional method. After the robot had been driven along the proposed test track, the robot's systematic errors were calibrated using Jung's method and conventional method, and the final position errors were compared.

Fig. 6 The experimental environment

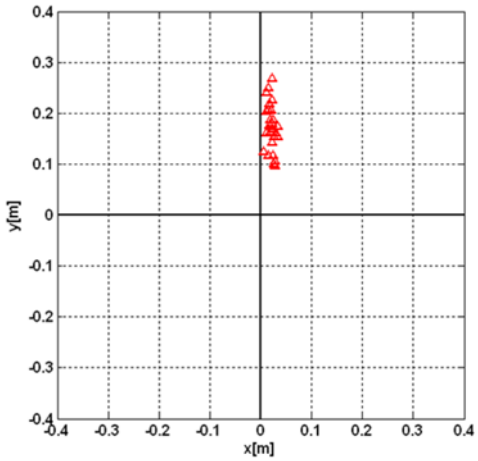

Fig. 7 The final pose errors after the test runs

5.1 Verification of the proposed method in practical environment

The initial test run was performed through a $4m \times 4m$ square path. The commercially available STARGAZER system was adopted to monitor the actual pose of the robot.[21] The test method was carried out to model the non-systematic errors.[18]

The experiment environment was a relatively smooth and flat floor as shown in Fig. 6. The robot was driven back and forth by an open-loop motion along a $10m$ straight-line path. The speed of the robot was approximately 0.2 *m/s*. To investigate the effect of non-systematic errors, the robot was driven 30 times under the same condition. The pose distribution around the center represents the stochastic non-systematic errors.

The final position and orientation errors during the test runs are plotted in Fig. 7. The results of the final position and orientation errors are listed in Table 2. The kinematic parameters estimated from the initial test runs along the predefined test track of the robot were $E_b = 0.980$ and $E_d = 0.992$. Based on the results, the non-systematic errors were modeled with the error constants of $k_r^{1/2} = 0.0013\ m^{1/2}$ and $k_l^{1/2} = 0.0013\ m^{1/2}$.

Fig. 8 shows the relative size of the orientation error caused by systematic errors over the total error. The relative orientation error caused by systematic errors over the total error increased with the straight-line length. The maximum value for a 4 m length was 90% considering the practical test space. Therefore, the proposed design of the test track can be summarized as a $4m \times 4m$ square path under the

Table 2 Experimental results of non-systematic error measurements by using the test method[18]

	x_{errors} (m)	y_{errors} (m)	θ_{errors} (°)
Mean (μ)	0.021	0.172	-1.05
Std. (σ)	0.007	0.046	1.48

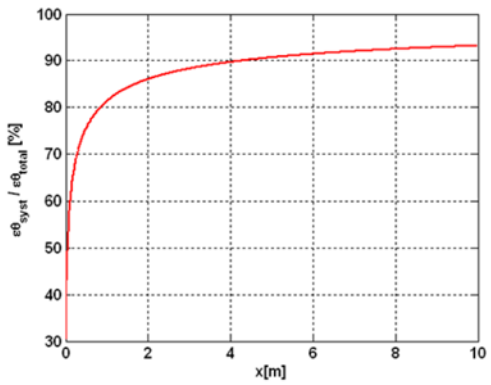

Fig. 8 The relative size of orientation errors caused by systematic errors compared with total orientation errors of the straight line path in test track

experimental conditions.

To show the advantage of the proposed design, the robot was driven along three different tracks. After open-loop motions in $2m \times 2m$, $4m \times 4m$, $6m \times 6m$ tracks, kinematic parameters were estimated using Jung's method. Table 3 represents the resultant error parameters.

Fig. 9 represents the mean and standard deviation of the final position errors after runs along the same $4m \times 4m$ square path in *CW* direction. When $2m \times 2m$ track was used, the final position errors were $2.01m$ on average. Under the use of the proposed method ($4m \times 4m$ track), the final position errors were $0.12m$, that is remarkably small. The final position errors after application of $6m \times 6m$ track were $0.13m$ on average. There are no significant changes in the final position errors between the mean of the final position error with $4m \times 4m$ and $6m \times 6m$ tracks.

Fig. 10 represents the mean and standard deviation of the final position errors after runs along the same regular triangular path with $5m$ edge in *CCW* direction. When $2m \times 2m$ track was used, the final position errors were $1.98m$ on average. Under the use of the proposed method ($4m \times 4m$ track), the final position errors were $0.07m$, that is remarkably small. The final position errors after application of $6m \times 6m$ track were $0.12m$ on average. There are no significant changes in the final position errors between the mean of the final position error with $4m \times 4m$ and $6m \times 6m$ tracks.

In order to investigate significant differences between the final position errors, statistical analysis was carried out using the independent samples *t-test*. Table 4 shows the independent samples *t-test* results of the final position errors shown in Fig. 9 for the equality of means of the proposed method ($4m \times 4m$ track) against the final position errors of $2m \times 2m$ and $6m \times 6m$ track sizes. In the first case ($2m \times 2m$ *vs.* $4m \times 4m$), the mean of the final position errors with the proposed method ($4m \times 4m$ track) was statistically different from the mean for $2m \times 2m$ track size at a significance level of 0.05 ($p < 0.05$). On the other hand, significance level p of the second case ($6m \times 6$m *vs.* $4m \times 4m$) was $0.927 > 0.05$. This fact implies that it is difficult to say that the difference

Table 3 Calibrated kinematic parameters

Error parameters	$2m \times 2m$	$4m \times 4m$	$6m \times 6m$
E_b	1.13702	1.02467	1.02127
E_d	1.00251	1.00162	1.00146

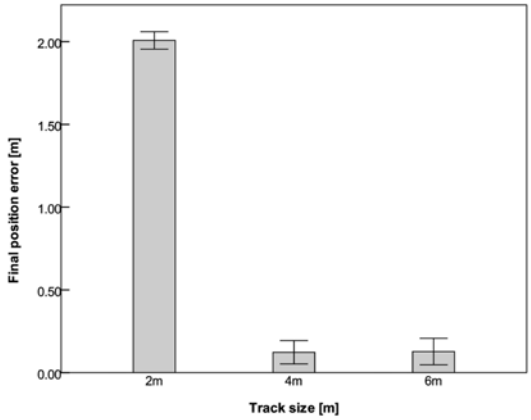

Fig. 9 Experimental final position errors when the robot is driven along $4m \times 4m$ square path in *CW* direction. Calibrations were carried out under different test track dimensions that are represented in x axis

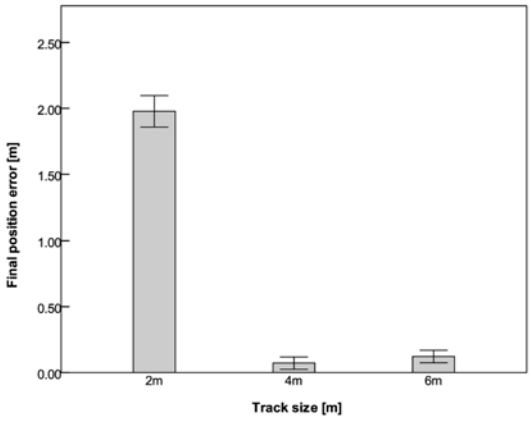

Fig. 10 Experimental final position errors when the robot is driven along regular triangular path with 5 m edge in *CCW* direction. Calibrations were carried out under different test track dimensions that are represented in x axis

Table 4 Results of independent samples *t-test* for equality of means of the proposed method ($4m \times 4m$) against that of different in square path

Case	t-value	Degree of freedom	p	Mean difference
$2m \times 2m$ vs. $4m \times 4m$	47.755	8	0.000	1.88470
$6m \times 6m$ vs. $4m \times 4m$	0.095	8	0.927	0.00454

between the mean of the final position errors with $4m \times 4m$ track and $6m \times 6m$ track is statistically meaningful.

Table 5 shows the independent samples *t-test* results of the final position errors shown in Fig. 10 for the equality of means of the proposed method ($4m \times 4m$ track) against the final position errors of $2m \times 2m$ and $6m \times 6m$ track sizes. As with the results shown in Table 4, the mean of the final position errors with the proposed method ($4m \times 4m$ track) was

Table 5 Results of independent samples *t-test* for equality of means of the proposed method ($4m \times 4m$) against that of different in triangular path

Case	t-value	Degree of freedom	p	Mean difference
$2m \times 2m$ *vs.* $4m \times 4m$	33.056	8	0.000	1.90629
$6m \times 6m$ *vs.* $4m \times 4m$	1.673	8	0.133	0.05037

Table 6 Resultant kinematic error parameters

Error parameters	UMBmark method	Proposed method
E_b	1.01503	0.99493
E_d	0.98249	0.98175

statistically different from the mean for $2m \times 2m$ track size at a significance level of 0.05 ($p < 0.05$) in the first case ($2m \times 2m$ *vs.* $4m \times 4m$). On the other hand, significance level p of the second case ($6m \times 6m$ *vs.* $4m \times 4m$) was $0.133 > 0.05$. This fact also implies that it is difficult to say that the difference between the mean of the final position errors with $4m \times 4m$ track and $6m \times 6m$ track is statistically meaningful. Therefore, $4m \times 4m$ track is preferable in practical environment owing to smaller experimental space.

5.2 Comparison with conventional method

The wheel diameter of the left wheel was intentionally increased by winding tape around the tire in order to create extreme situations. The approximate difference in wheel diameter between the two wheels was 2.5~3.0*mm*. The robot was driven by open-loop motion along the proposed test track ($4m \times 4m$ track) in the *CW* and *CCW* directions. To reduce the effect of non-systematic errors, the robot was driven five times. The experimental heading errors of the robot were measured using a commercially available gyro sensor.[22] The error of the heading angle was less than $0.04^{\circ}/s/\sqrt{Hz}$ at $\pm 150^{\circ}/s$ spot-rotation. The robot's initial and final poses were used for the calibration process according to conventional UMBmark and Jung's method.

On average, the final position errors before calibration were 1.94*m* and 2.54*m* in the *CW* and *CCW* directions, respectively, and the robot's final orientation errors were -51.3° and -36.4° in the *CW* and *CCW* directions, respectively. The experimentally measured standard deviation of the gyro sensor's heading angle was smaller than 0.2. Non-systematic errors of the calibration experiments were significantly larger than that for the standard deviation of the heading angle of the gyro sensor. Therefore, the robot's final heading errors were useful for estimating the kinematic parameters. Based on the final position and orientation errors, the kinematic parameters E_b and E_d were estimated and compensated. The resultant error parameters from the experiments are listed in Table 6.

The experimental results are presented in Fig. 11 and Table 7. After application of the conventional UMBmark, the final position errors were reduced to 0.35*m* on average. The final position errors after application of the proposed scheme were 0.07*m* on average in both directions. The odometry accuracy of the proposed scheme was five times higher than that of the conventional approach. This result clearly shows the advantage of using the proposed scheme with a commercially available gyro sensor over the prior approach.

In order to investigate the advantage of accurate calibration, it is

Table 7 Results of the odometry accuracy after calibration

Experiment	Final Position Errors (m)			
	Uncalibrated odometry	UMBmark method	Proposed method	Improvement
CW	1.94	0.37	0.05	
CCW	2.54	0.32	0.08	
Average	2.24	0.35	0.07	5 times

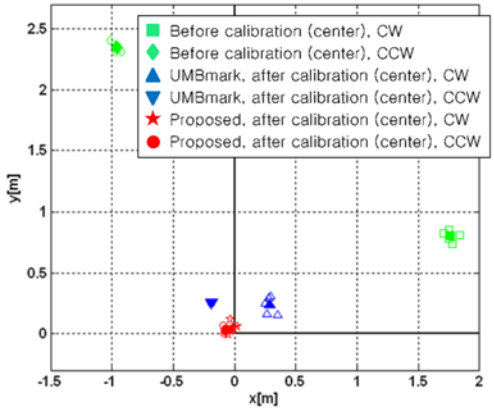

Fig. 11 Comparison between the proposed and the conventional UMBmark methods. The final position errors of the proposed scheme are smaller

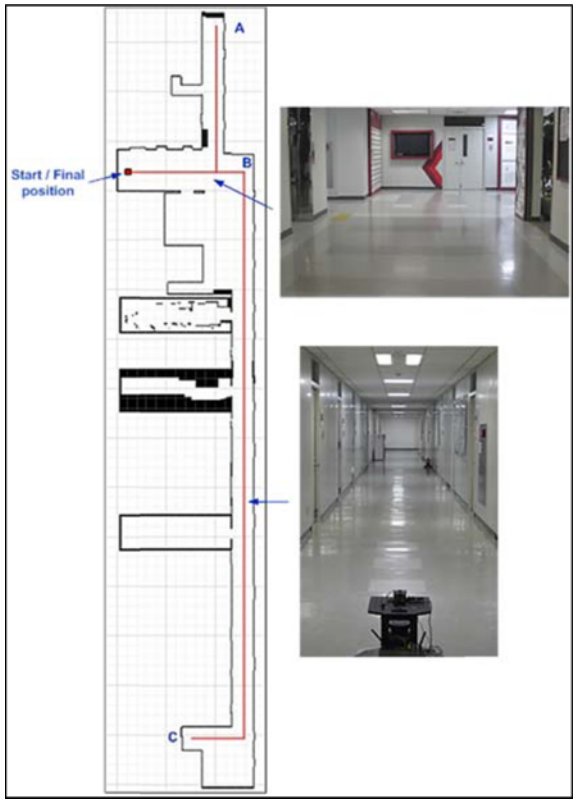

Fig. 12 The indoor hallways for mapping using odometry

useful to build maps on the basis of pure odometry. Fig. 12 shows an experimental environment and a reference path. A mobile robot moves along the corridor of an office building. A map is built by registration of range measurements from a laser range finder (SICK LMS 200). The

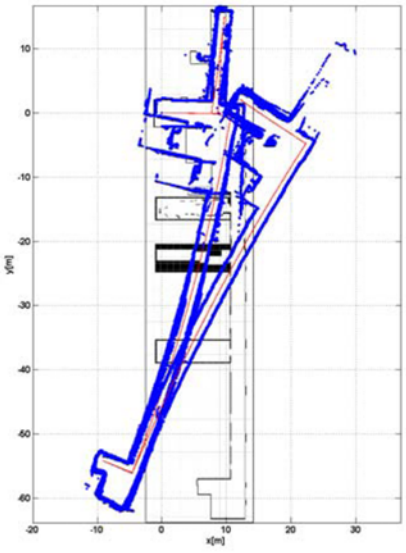

(a)

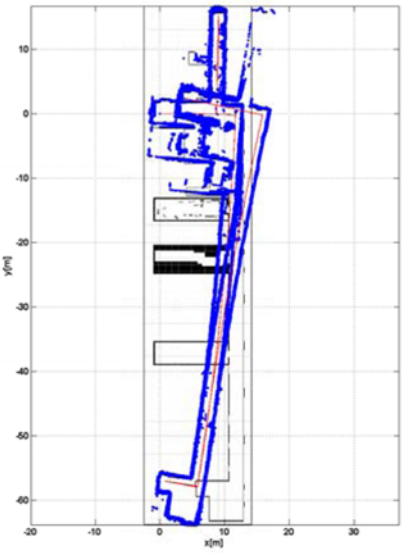

(b)

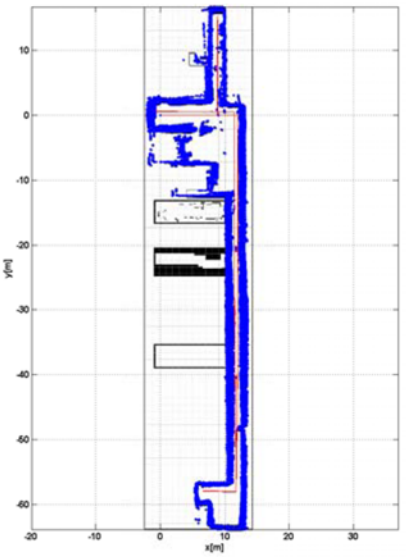

(c)

Fig. 13 Results of the constructed maps by the two wheel differential mobile robot. (a) is an odometry map, (b) is a map by the UMBmark method and (c) is a map by the proposed method

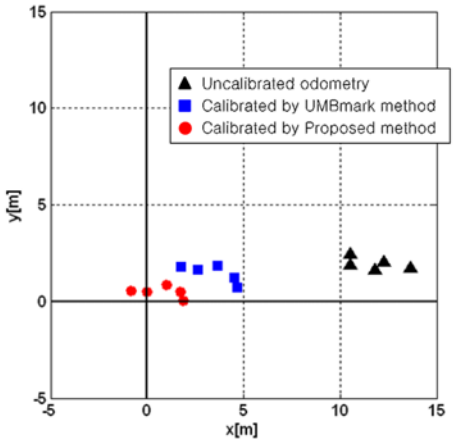

Fig. 14 Results of the final position errors after navigation with two wheel differential mobile robot

Table 8 Results of independent samples *t-test* for equality of means of the proposed method against that of uncalibrated odometry and UMBmark method

Case	t-value	Degree of freedom	*p*	Mean difference
Uncalibrated vs. Proposed	17.21	8	.000	10.601
UMBmark vs. Proposed	4.974	8	.001	2.530

traveling distance of a robot was approximately 180*m*.

Three experimental maps by pure odometry are shown in Fig. 13. Fig. 13(a) shows the map before calibration. The map after application of the conventional UMBmark is shown in Fig. 13(b). The resultant map by the proposed scheme is shown in Fig. 13(c). From Fig. 13, it is evident that the proposed scheme resulted in the most accurate map.

It is significant to evaluate the improved performance from the viewpoint of statistical analysis. Each experiment in Fig. 13 has been carried out for five times. Under the same boundary conditions, the final position errors have been monitored as shown in Fig. 14. The mean errors of the uncalibrated odometry and the conventional UMBmark were 11.90*m* and 3.83*m*, respectively. The mean error of the proposed scheme was 1.30*m* that shows the superior accuracy of the proposed calibration scheme.

Statistical analysis was carried out by using the independent samples *t-test* to verify significant differences between the means of the final position errors. Table 8 shows the independent samples t-test result of the final position errors for equality of means of the proposed method against those of uncalibrated odometry and UMBmark. As shown in Table 8, odometry corrected by the proposed method had a different mean with a significance level of 0.05 ($p < 0.05$). Therefore, the improvement in odometry accuracy by the proposed method is statistically efficient with a significance level probability of 0.05. The details of experimental calibration were introduced in.[13]

6. Conclusions

We have proposed design guidelines for a test track to calibrate odometry. The shape and size of the test track play a significantly role

in calibration experiments because the systematic errors are reflected in the pose errors. The test track should be carefully determined to consider the experimental space, wheel diameter, calibration equations, and systematic and non-systematic errors. Based on the design considerations, a test track is recommended to have a regular polygonal path. Considering the experimental space, the proposed test track was designed to have the shape of a square path. The relative sizes of the orientation error caused by systematic errors over the total orientation error were compared to determine the appropriate track size for a practical experimental space. The proposed scheme was experimentally verified, and its advantages were clearly demonstrated through a quantitative comparison.

ACKNOWLEDGEMENT

This work was supported by the National Research Foundation of Korea (NRF) grant funded by the Korea government (MEST) (2013-029812). This research also was supported in part by the MKE(The Ministry of Knowledge Economy), Korea, under the Human Resources Development Program for Convergence Robot Specialists support program supervised by the NIPA (National IT Industry Promotion Agency) (NIPA-2013-H1502-13-1001). The research was also supported by the Implementation of Technologies for Identification, Behavior, and Location of Human based on Sensor Network Fusion Program through the Ministry of Knowledge Economy (Grant Number: 10041629).

REFERENCES

1. Dugarjav, B., Lee, S. G., Kim, D., Kim, J., and Chong, N., "Scan Matching Online Cell Decomposition for Coverage Path Planning in an Unknown Environment," Int. J. Precis. Eng. Manuf., Vol. 14, No. 9, pp. 1551-1558, 2013.
2. Kim, J., Woo, S., Kim, J., Do, J., Kim, S., and Bae, S., "Inertial Navigation System for an Automatic Guided Vehicle with Mecanum Wheels," Int. J. Precis. Eng. Manuf, Vol. 13, No. 3, pp. 379-386, 2012.
3. Cheng, P. Y. and Chen, P. J., "Navigation of Mobile Robot by using D++ Algorithm," Intelligent Service Robotics, Vol. 5, No. 4, pp. 229-243, 2012.
4. Bashiri, M., Vatankhah, H., and Shiry Ghidary, S., "Hybrid Aaptive Dfferential Evolution for Mobile Robot Localization," Intelligent Service Robotics, Vol. 5, No. 2, pp. 99-107, 2012.
5. Thrun, S., Burgard, W. and Fox. D., "Probabilistic Robotics," The MIT Press, pp. 39-147, 2005.
6. Borenstein, J. and Feng, L. "Measurement and Correction of Systematic Odometry Errors in Mobile Robots," Proc. of. IEEE Transactions on Robotics and Automation, vol. 12, no. 6, pp. 869-880, 1996.
7. Siegwart, R., Nourbakhsh, I.R. and Scaramuzza, D. "Introduction to Autonomous Mobile Robots," The MIT Press, pp. 265-367, 2011.
8. Bento, L. C., Nunes, U., Moita, F. and Surrecio, A., "Sensor Fusion for Precise Autonomous Vehicle Navigation in Outdoor Semi-structured Environments," Proc. of IEEE International Conference on Intelligent Trasportation System, pp. 245-250, 2005.
9. Surrécio, A., Nunes, U. and Araujo, R. "Fusion of Odometry with Magnetic Sensors Using Kalman Filters and Augmented System Models for Mobile Robot Navigation," Proc. of IEEE International Symposium on Industrial Electronics, Vol. 4, pp. 1551-1556, 2005.
10. Komoriya, K. and Oyama, E., "Position Estimation of a Mobile Robot Using Optical Fiber Gyroscope (OFG)," Proc. of IEEE International Conference on Intelligent Robots and Systems, Vol. 1, pp. 143-149, 1994.
11. Martinelli, A., "The Odometry Error of a Mobile Robot with a Synchronous Drive System," Proc. of IEEE Transactions on Robotics and Automation, Vol. 18, No. 3, pp. 399-405, 2002.
12. Martinelli, A., Tomatis, N., and Siegwart, R., "Simultaneous Localization and Odometry Self Calibration for Mobile Robot," Autonomous Robots, Vol. 22, No. 1, pp. 75-85, 2007.
13. Antonelli, G., Chiaverini, S. and Fusco, G., "A Calibration Method for Odometry of Mobile Robots Based on the Least-Squares Technique: Theory and Experimental Validation," Proc. of IEEE Transactions on Robotics, Vol. 21, No. 5, pp. 994-1004, 2005.
14. Antonelli, G. and Chiaverini, S., "Linear Estimation of the Physical Odometric Parameters for Differential-Drive Mobile Robots," Autonomous Robots, Vol. 23, No. 1, pp. 59-68, 2007.
15. Censi, A., Marchionni, L. and Oriolo, G., "Simultaneous Maximum-Likelihood Calibration of Odometry and Sensor Parameters," Proc. of IEEE International Conference on Robotics and Automation, pp. 2098 – 2103, 2008.
16. Antonelli, G., Caccavale, F., Grossi, F., and Marino, A., "A Non-Iterative and Effective Procedure for Simultaneous Odometry and Camera Calibration for a Differential Drive Mobile Robot Based on the Singular Value Decomposition," Intelligent Service Robotics, Vol. 3, No. 3, pp. 163-173, 2010.
17. Jung, C. and Chung, W. "Accurate Calibration of Two Wheel Differential Mobile Robots by Using Experimental Heading Errors," Proc. of IEEE International Conference on Robotics and Automation, pp. 4533-4538, 2012.
18. Chong, K. S. and Kleeman, L. "Accurate Odometry and Error Modelling for a Mobile Robot," Proc. of IEEE International Conference on Robotics and Automation, No. 4, pp. 2783-2788, 1997.
19. Dongbu Robot Co. Ltd., "Tetra-DS Operation Manual V1.0," 2009.
20. Peck, R., Olsen, C., and Devore, J. L., "Introduction to Statistics and Data Analysis," Cengage Learning, 4th Ed., pp. 638-658, 2011.
21. Hagisonic Co. Ltd., "StarGazer_Guide.02.090416," 2010.
22. Xsens Co. Ltd., "MTi and MTx User Manual and Technical Documentation," http://projects.asl.ethz.ch/datasets/lib/exe/fetch.php?media=hardware:tiltinglaser:mti-g_user_manual_and_technical_documentation.pdf (Accessed 10 Dec 2013)